



Magnetic fabrics of diamagnetic rocks and the strain field associated with the Dead Sea Fault, northern Israel

Tsafrir Levi*, Ram Weinberger

Geological Survey of Israel, 30 Malkhe Israel St., Jerusalem 95501, Israel

ARTICLE INFO

Article history:

Received 23 June 2010

Received in revised form

3 February 2011

Accepted 13 February 2011

Available online 19 February 2011

Keywords:

Anisotropy of magnetic susceptibility

Diamagnetism

Structural geology

Dead Sea Fault

ABSTRACT

In order to exploit the potential of AMS axes (k_1 , k_2 , k_3) and magnitudes as a tool to estimate the strain field around major faults, the AMS of calcite-bearing diamagnetic rocks that crop out next to the Dead Sea Fault (transform) (DSF) were measured. The calcite-bearing Bar Kokhba limestone contains magnetic fabrics due mainly to the diamagnetic phase, as indicated by the low iron content (<130 ppm), and strong negative susceptibilities of all the AMS principal axes. The magnetic fabrics are solely controlled by the alignment of c -axes of almost pure calcite crystals and help to assess the strain fields prevailing post-deposition and during the tectonic evolution of the DSF. Based on the AMS measurements of 146 diamagnetic samples as well as 65 paramagnetic samples, three groups of minimum k_3 AMS axes are defined: (1) ~NNE-plunging axis; (2) ~NW–SE axis; and (3) ~E–W axis. The latter two groups of k_3 axes are aligned sub-parallel to Neogene to Pleistocene finite-strain axes inferred from meso-scale structures (i.e., folds, faults and veins) next to the DSF. This indicates that k_3 axes of diamagnetic rocks can be excellent proxies for strain field directions around major faults. Differences in the degree of anisotropy P' (up to ~2%) and in susceptibility difference Δk (up to ~0.2) of the diamagnetic rocks are related to differences in strain magnitudes. Based on the proximity of the studied outcrops to the fault traces, the values of these variables reflect the stored inelastic strain within the calcite matrix due to repeated faulting activity.

© 2011 Elsevier Ltd. All rights reserved.

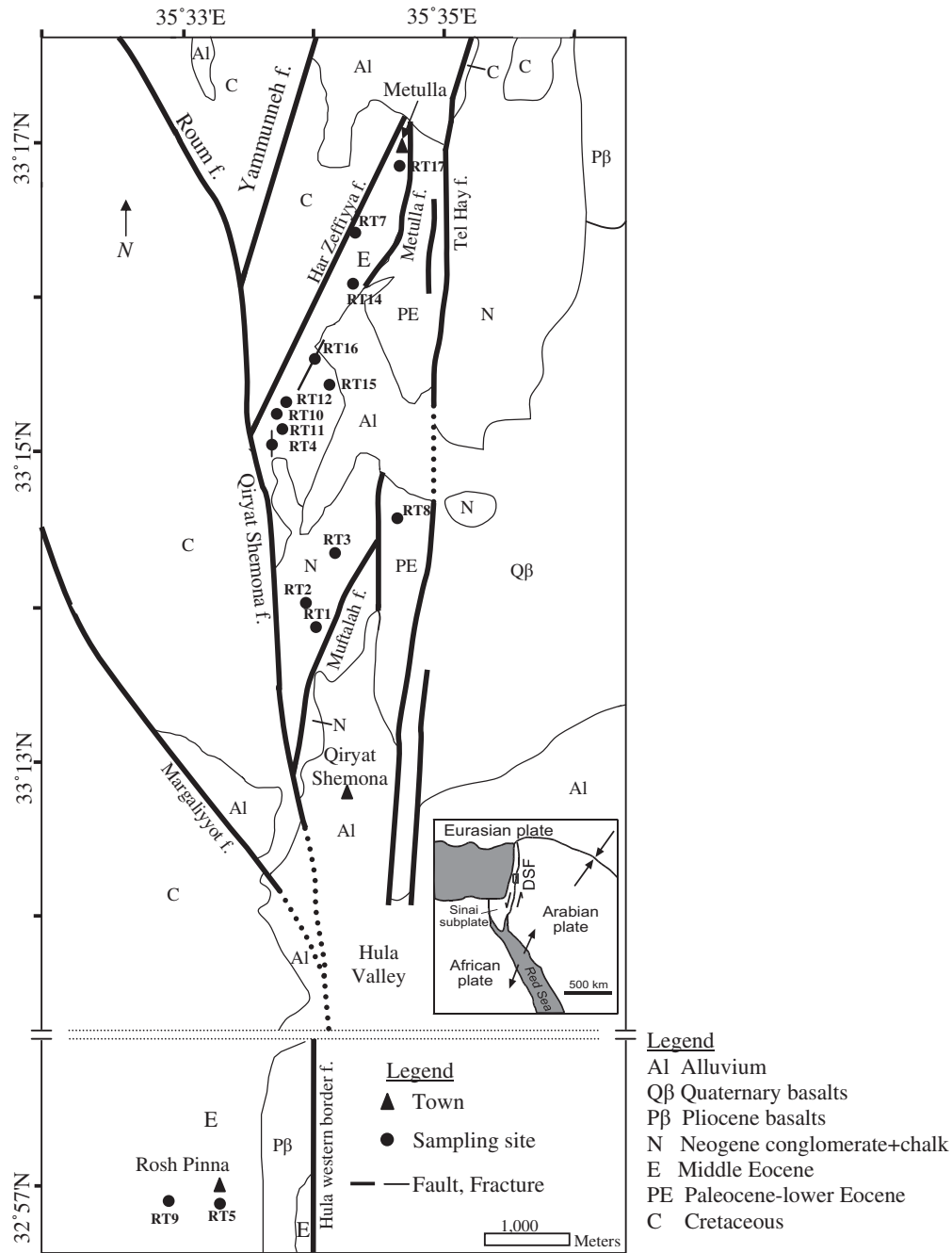
1. Introduction

The magnetic susceptibility of rocks results from the combined contribution of ferromagnetic, paramagnetic, and diamagnetic sub-fabrics/components. Minerals that are the source of the three sub-fabrics are commonly magnetically anisotropic, depending on their preferred crystallographic orientation or grain shape. This gives rise to the Anisotropy of Magnetic Susceptibility (AMS) of rocks, which provides a petrofabric tool by averaging out the orientation-distribution of all minerals and ferromagnetic, paramagnetic, and diamagnetic sub-fabrics in a rock specimen (Raposo et al., 2006; Borradaile and Jackson, 2010). AMS has been used as an indicator for flow directions in sediments (Tarling and Hrouda, 1993; Liu et al., 2001), injection structures (Levi et al., 2006a,b), and magmas (Baer, 1995; Abelson et al., 2001); and has also been correlated with strain in rocks (Borradaile, 1991; Parés et al., 1999; Parés and Van der Pluijm, 2003). In order to better understand the relation between AMS and rock deformation, it is necessary to

isolate the AMS contributions of certain minerals and sub-fabrics from one another (e.g., Evans et al., 2003; Almqvist et al., 2009, 2010). Calcite-bearing rocks are abundant in many sedimentary environments and tectonic settings, but their AMS has rarely been examined due to their weak diamagnetic susceptibility (de Wall et al., 2000). With the advance in laboratory instruments and techniques, the AMS of calcite and monomineralitic calcite-bearing rocks can accurately and reproducibly be measured (Schmidt et al., 2006). We extended the use of diamagnetic AMS as a petrofabric tool and strain indicator in calcite-bearing rocks, isolating the AMS axes and magnitudes in rocks that crop out next to the plate-boundary Dead Sea Fault (transform) in northern Israel. The Dead Sea Fault (DSF) accommodates the relative left-lateral motion between the Arabian plate and Sinai subplate. In the study area it branches into at least five major faults, forming highly deformed structural blocks. In these blocks, the transpression along the DSF has been partitioned into strike-slip and contractional domains since the Pleistocene (Weinberger et al., 2009). Revealing the spatial and temporal variations of the strain field and its partitioning within the deformed blocks provides insight into the tectonic evolution of plate boundaries. We compared the orientations of

* Corresponding author.

E-mail address: tsafrir@gsi.gov.il (T. Levi).



Legend
 Al Alluvium
 Qβ Quaternary basalts
 Pβ Pliocene basalts
 N Neogene conglomerate+chalk
 E Middle Eocene
 PE Paleocene-lower Eocene
 C Cretaceous

Fig. 1. Geological map of the Dead Sea Fault (DSF) in the study area. Names of faults are marked. Circles mark the sampling sites. The inset shows the plate tectonic configuration resulting in left-lateral motion across the DSF (after Sneh and Weinberger, 2003b). C – Cretaceous; PE – Paleocene–Eocene; E – Eocene; N – Neogene; Pβ – Pliocene basalts; Qβ – Quaternary basalts; Al – Aluvium.

AMS and finite-strain axes obtained from meso-scale structures, and discuss the structural significance of the AMS magnitudes.

2. AMS, rock deformation, and susceptibility of calcite

Magnetic susceptibility indicates the capacity of material to be magnetized in an applied magnetic field. In anisotropic material the magnetic susceptibility (*k*) relates the applied magnetic field (*H*) to an induced magnetization (*M*) in a sample by $M_{ij} = k_{ij}H_j$. The shape of the AMS is described by the three principal values $k_{max}(k_1)$, $k_{int}(k_2)$, and $k_{min}(k_3)$, which correspond to the maximum, intermediate and

minimum magnetic susceptibility magnitudes, respectively (Borradaile and Jackson, 2004). There is a wide variety of parameters that have been used to describe the axial magnitude relationships of the susceptibility ellipsoid. The simplest expressions are the mean susceptibility, $k_m = (k_1 + k_2 + k_3)/3$, the degree of AMS, $P = k_1/k_3$, the ‘corrected anisotropy degree’, P' (for more details see Jelínek, 1981), the susceptibility difference ($\Delta k = k_1 - k_3$) (Jelínek, 1981), the magnetic lination, $L = k_1/k_2$, the magnetic foliation, $L = k_2/k_3$, and the degree of ellipsoid shape, $T = 2[\ln k_2 - \ln k_3]/[\ln k_1 - \ln k_3] - 1$, measuring the range from prolate ($T < 0$) through sphere ($T = 0$) to oblate ($T > 0$) ellipsoids (Jelínek, 1981).

AMS is a second-rank tensor, leading to attempts of correlating AMS and strain (e.g., Kligfield et al., 1982; Borradaile, 1987, 1991; Hrouda, 1993; Hirt et al., 2000). In most deformed environments, the directions of the AMS axes show a fair to good correlation with the directions of the principal strain axes (e.g., Borradaile, 1987, 1988, 1991; Tarling and Hrouda, 1993; Borradaile and Henry, 1997; Parés et al., 1999; Latta and Anastasio, 2007; Soto et al., 2007; Mamtani and Sengupta, 2008; Hrouda et al., 2009; Burmeister et al., 2009). When tectonic foliation is present, the principal AMS axes parallel the flattening plane of the finite-strain ellipsoid, with the minimum axes perpendicular to foliation and the maximum AMS axes typically parallel to the tectonic extension direction or to the intersection of bedding and cleavage (Parés and Van der Pluijm, 2003 and references therein).

Success has been limited and no reliable correlation between the magnitudes of the AMS axes and those of strain magnitudes has been established (e.g., Parés and Van der Pluijm, 2004; Latta and Anastasio, 2007; Borradaile and Jackson, in press; Tripathy et al., 2009). This is mainly because the magnitudes of the AMS axes are more complexly related to finite strain. One major cause for the unsuccessful attempt to correlate magnitudes of the AMS axes and magnitudes of strain axes is that the former are mainly governed by the percentage of the Fe and Mn-minerals bearing in the rock (Borradaile and Henry, 1997; Schmidt et al., 2006). Furthermore, strongly aligned minerals that are produced by stress-controlled crystallization have a maximum AMS that cannot increase with strain. Valid correlations between AMS and strain generally require that maximum shortening be greater than 30%, so that primary AMS fabrics are obliterated. In most cases when the mean susceptibility, k_m , and the corrected anisotropy degree, P' , were increased, the increases of these AMS parameters were attributed to the increases in Fe and Mn mineral contents and not to the magnitude of strain.

A pure calcite crystal is magnetically anisotropic with susceptibility values of $k_3 = -13.2 \times 10^{-6}$ (SI) along the c -axis, $k_1 = -12.09 \times 10^{-6}$ (SI) along the ab plane, $k_m = -12.47 \times 10^{-6}$ (SI) and is considered to be oblate (after Schmidt et al., 2006). The redistribution of calcite c -axes is associated with applied stress or incremental strain in experiments (Casey et al., 1978); the c -axes are aligned parallel to the compression direction. The AMS of the diamagnetic fraction in calcite-bearing rocks should be lower than the anisotropy of single crystals or deformed calcite-bearing rocks because perfect alignments are rare, especially in sedimentary rocks (Hrouda, 2004 and references therein). Calcite twinning and other crystal-plastic deformations (e.g., Evans and Elmore, 2006) have long been used in petrofabric studies as sensitive indicators of incremental strain axes and are essentially parallel to the causative paleo-stress axes (Borradaile and Hamilton, 2004; Hamilton et al., 2004 and references therein). Hence calcite is considered one of the most reliable stress (strain)-sensitive petrofabric indicators (Borradaile and Jackson, 2004).

During the sedimentation process some of the c -axes can be parallel to the lithostatic pressure, depending on the pressure magnitude (Hrouda, 2004). In such a case, the k_1 and k_2 axes would be parallel to the bedding plane and the k_3 axes would group vertically to the bedding plane and parallel to the minimum strain axis (Z). During shortening or elongation (extension) regimes the AMS axes are generally parallel to the principal strain directions ($X \geq Y \geq Z$), where X is the maximum elongation, Y is the intermediate strain axis and Z is the maximum shortening. Under these conditions, generally $k_1 \parallel X$, $k_2 \parallel Y$, $k_3 \parallel Z$, and the AMS fabric is 'normal' ($k_3 \parallel c$ -axes) (e.g., Borradaile and Jackson, 2010).

Calcite becomes less diamagnetic or even paramagnetic with the addition of Fe^{2+} and Mn^{2+} ions (Rochette, 1988; Rochette et al., 1992; Schmidt et al., 2006; Schmidt et al., 2007; Almqvist et al.,

2009; Borradaile and Jackson, 2010). In cases where the substitution of Fe^{2+} and Mn^{2+} for Ca^{2+} is more than 400 ppm (iron-rich calcite) (Schmidt et al., 2006), 'an inverse' ($k_1 \parallel c$ -axes) AMS fabric is produced (Rochette, 1988; Ihlmlé et al., 1989) and represented by a prolate AMS ellipsoid (Schmidt et al., 2006).

3. Tectonic and geological setting

Between the Gulf of Eilat (Aqaba) and southern Lebanon, the major strands of the DSF step left along a north–south axis. Due to the left-lateral motion along these strands, they are associated with the formation of several basins, one of which is the Hula basin (Fig. 1). Farther north in Lebanon, the Yammuneh master fault veers north-northeastward, corresponding to a restraining geometry that uplifted the Lebanon and Anti-Lebanon mountains (Beydoun, 1977; Daeron et al., 2004). The transition of the DSF from the Hula basin to the Lebanese restraining bend is complex, with deformation distributed across a zone of several faults and deformed structural blocks (Picard, 1952; Glikson, 1966). The Qiryat Shemona fault is considered the main strand of the DSF in this area (Sneh and Weinberger, 2003a). It subdivides the highly deformed contraction area into two main blocks; a western block, between the Qiryat Shemona and Margaliyyot faults, locally known as the Misgav Am block; and an eastern block, between the Qiryat Shemona and Tel-Hay faults, locally known as the Metulla block (Fig. 1).

The eastern (Metulla) block is the main focus of the present study. The block is ~2 km wide and is divided into several moderate to highly deformed sub-blocks by ~NE–SW to N–S striking faults, including the Har Zefiyya, Metulla, Muftalah and Kefar Giladi faults (Fig. 1). Strata exposed in this block consist of the Cretaceous Kamon and Deir Hanna formations, the Paleocene Taqiye Formation, the Eocene Timrat and Bar Kokhba formations, the Neogene Kefar Giladi Formation, the Pleistocene Hazbani Basalt and Quaternary gravels and clays. The conglomerates and lacustrine sediments of the Kefar Giladi Formation are especially noteworthy because they accumulated within an extensional basin adjacent to the DSF and were subsequently uplifted and folded during the Pleistocene (Weinberger et al., 2009). In the south, on both sides of the NE-striking Muftalah fault, the Kefar Giladi beds are vertical and in places intensely contorted. The NE–SW striking Har Zefiyya fault dips ~70° southeastward, showing normal separation with the Eocene Bar Kokhba limestone in the hanging wall and the Cenomanian Karkara beds exposed in the footwall. Kinematic indicators (dip-slip striae lineations and small-scale pull-apart basins filled with calcite) suggest a younger reverse motion along this fault.

Based on structural and kinematic analyses (i.e., folds, faults, veins) within the western and the eastern blocks, Weinberger et al. (2009) suggested that two directions of regional shortening exist: (1) ~NW–SE shortening responsible for the formation of ~NE–SW trending fold axes and a left-lateral strike-slip motion along the N–S trending faults; and (2) ~E–W shortening as indicated by N–S trending fold axes, N–S striking thrust faults and extensional ~E–W striking calcite-filled veins. Based on cross-cutting relations and late-Pleistocene U–Th ages of the calcite-filled vein, they suggested that the ~E–W phase of transform-normal shortening post dates the NW–SE of shortening. In addition, they suggested that transition occurred from an early (Miocene–Pliocene) phase of pure strike-slip motion to a late (Plio?–Pleistocene to Recent) phase of convergent strike slip of "partitioned" transpression. The latter is characterized by discrete left-lateral strike-slip motion across weak N–S faults and the development of a fold-thrust belt in response to transform-normal shortening.

Table 1
General information on the sampling sites.

Sampling site	Location	No. (all)	Stratigraphic unit	Structure type	Mean susceptibility ($k_m, \times 10^{-6}$ (SI))	Anisotropy degree (P')	Susceptibility difference $k_1 - k_3$ ($\Delta k, \times 10^{-6}$ (SI))	Shape parameter (T)
RT1	25319E/79262N	22	Kefar Giladi Fm. (Neogene, chalk)	Fold	42.67	1.02	0.902	-0.31
RT2 (SE flank)	25309E/79271N	19	Kefar Giladi Fm. (Neogene, chalk)	Fold	15.1	1.015	0.24	0.02
RT2 (SW flank)	25309E/79271N	7	Kefar Giladi Fm. (Neogene, chalk)	Fold	12.3	1.019	0.134	0.08
RT3 (NW flank)	25396E/79367N	11	Kefar Giladi Fm. (Neogene, chalk)	Fold	38.5	1.01	0.378	-0.21
RT3 (SE flank)	25396E/79367	6	Kefar Giladi Fm. (Neogene, chalk)	Fold	39.5	1.012	0.422	0.06
RT4	25296E/79461N	28	Bar Kokhba Fm. (Middle Eocene, limestone)	Fault plane	-10.1	1.016	0.149	0.04
RT5	25054E/26198N	16	Bar Kokhba Fm. (Middle Eocene, limestone)	Fold	-8.45	1.014	0.114	0.57
RT7	25384E/79769N	10	Bar Kokhba Fm. (Middle Eocene, limestone)	Fold-Near Fault plane	-8.53	1.024	0.197	0.76
RT8	25427E/79364N	16	Timrat Fm. (Lower Eocene, limestone)	Fold	7.43	1.011	0.093	-0.06
RT9	24926E/76204N	12	Bar Kokhba Fm. (Middle Eocene, limestone)	Near Fault plane	-12.6	1.008	0.114	0.58
RT10	25266E/79487N	14	Bar Kokhba Fm. (Middle Eocene, limestone)	Near Fault plane	-7.86	1.014	0.114	-0.03
RT11	25277E/79485N	15	Bar Kokhba Fm. (Middle Eocene, limestone)	Near Fault plane	-7.28	1.005	0.075	0.23
RT12	25258E/79522N	13	Bar Kokhba Fm. (Middle Eocene, limestone)	Near Fault plane	-10.72	1.008	0.116	0.2
RT14	25374E/79703N	15	Bar Kokhba Fm. (Middle Eocene, limestone)	Center of Metulla block	-10.28	1.007	0.105	0.1
RT15	25355E/79576N	16	Bar Kokhba Fm. (Middle Eocene, limestone)	Center of Metulla block	-9.59	1.007	0.082	0.05
RT16	25314E/79619N	12	Bar Kokhba Fm. (Middle Eocene, limestone)	Fault plane	-7.46	1.015	0.101	0.12
RT17	25417E/79780N	14	Bar Kokhba Fm. (Middle Eocene, limestone)	Center of Metulla block	-12.55	1.004	0.081	-0.03
RT18	25296E/79442N	7	Calcite-filled vein	Vein	-11.89	1.075	0.114	0.84

4. Methods and sampling strategy

4.1. Low-field AMS and rock magnetism

The tectonic significance of weak susceptibilities requires special consideration (Hamilton et al., 2004), particularly when working with AMS data of diamagnetic rocks such as the Eocene Bar Kokhba limestone. The AMS was measured with a KLY-4S Kappabridge at the Geological Survey of Israel (GSI) laboratory. The sensitivity of the kappabridge is in the order of 1×10^{-8} (SI), enabling measurements of the mean susceptibility of samples on a 1×10^{-6} (SI) order. The measurements were repeated several times in a low magnetic field of 300 A/m. Because the magnetic signal in the diamagnetic rocks is low and the magnetic difference ($\Delta k = k_1 - k_3$) may be close to the measurement error of the directional susceptibility (Hrouda et al., 2000), we tested the significance of the AMS anisotropy by applying statistical F -tests (Jelinek, 1977), where for 95% and 90% confidences the F -test should be higher than 4.2 and 3.0, respectively. If a specimen had axes with positive and negative susceptibilities, it was omitted from further analysis. This was done because the AMS is carried by both diamagnetic and paramagnetic sub-fabrics, which may lead to wrong interpretations (Hamilton et al., 2004; Hrouda, 2004). Samples that have k_m in range of -4 to 4×10^{-6} (SI) were also omitted from further analysis because of an unrealistic high degree of P' in the vicinity close to zero susceptibility (Hrouda, 2004).

The ellipsoid shape parameters and the AMS confidences were derived according to Jelinek's (1981) procedure and Hrouda (2004). The AMS magnitudes and the directions of the AMS principal axes were calculated using the software package *Anisoft3*.

In this study the AMS axes of diamagnetic rocks are described by assigned values of susceptibility. Therefore, the minimum susceptibility (k_3) refers to the most negative susceptibility value, which coincides with the crystallographic c -axis in calcite (Almqvist et al., 2009). In addition, the AMS parameters (P, P', L, F, T) are calculated based on the absolute (unsigned) values of the principal susceptibility, which means that the largest absolute magnitude is the maximum susceptibility. This convention is recommended for describing the orientations of the principal axes and their magnitudes (for more details see Hrouda, 2004).

For the AMS study a total of 223 samples were taken from 17 outcrops within the eastern (Metulla) block, 7–26 from each outcrop (Fig. 1; Table 1). Most of the rocks sampled are the Bar Kokhba limestone (12 sites), a few are chalks of the Timrat and Kefar Giladi formations (4 sites), and one sample is from a late-Pleistocene calcite-filled vein. Several sites were chosen because they were located along fault planes that are part of the Qiryat Shemona and Har Zefiyya fault zones; others because they were located away from these faults (Fig. 1). Folded and highly tilted beds were also sampled.

4.2. Rock magnetism

Several rock-magnetic experiments were carried out at the rock-magnetic laboratories in the Institute of Earth Sciences, Hebrew University (HU) of Jerusalem, and the Geological Survey of Israel (GSI), Jerusalem. These experiments were done in order to define the magnetic carriers and their contribution to the mean magnetic susceptibility and its anisotropy. The remanent magnetization was measured using a three-axis 2G Enterprises superconducting magnetometer with integrated alternating field (AF) coils at the HU. The anisotropy of anhysteresis remanent magnetization (AARM) was investigated by imparting magnetization along six chosen directions in an alternating field of 100 mT with a small coaxial field of 80 μ T. Low-field thermomagnetic measurements in an Ar atmosphere were conducted by using a CS-3 apparatus coupled to

Table 2
Chemical content (the results are in ppm, except Ca⁺) and composition from LA-ICP-MS.

Sample	Ca ⁺	Mg	Na	v	Cr	Mn	Fe	Ni	Cu	Sr	Ba	Pb	Tb
RT1-3b	35	1050	45	10	8	70	545	4	30	50	16	1.9	0.16
RT2-3b	38.3	1150	15	4	3	100	900	3	35	95	17	0.4	0.02
RT3-3	34	2100	85	8	12	130	750	≤1	35	110	36	1.7	0.17
RT4-11	39.5	900	15	3	7	20	95	3	900	106	3.8	0.5	5
RT7-3	39.1	1350	90	6	19	15	125	2	60	120	2.5	0.4	0.06
RT9-3	39.4	1350	30	15	14	4	50	3	40	260	2.5	0.2	0.02
RT10-2	39.2	4500	≤10	≤1	5	24	130	2	30	15	2	0.3	0.01
RT14-14	39.3	400	25	2	2	12	63	≤1	100	20	2.6	0.2	0.07
RT16-6	39.2	550	25	5	11	13	38	3	50	40	2	0.3	0.1
RT17-2	40	780	≤10	≤1	4	27	47	2	20	33	1.7	0.3	0.02

the KLY-3S Kappabridge instrument at the GSI. For more details see [Supplementary data item #1](#).

4.3. Chemical composition

Magnetic fabrics of calcite rocks may be affected by the content of Fe²⁺ and Mn²⁺ ions, mainly when the samples consist of more than 500 ppm Fe and Mn (Schmidt et al., 2006). To test the possibility of Fe and Mn contributions to the magnetic fabrics, the chemical composition of ten samples was analyzed by Inductively Coupled Plasma Mass Spectrometer (ICP-MS) at the Geological Survey of Israel (GSI). Based on this method all elements with possible paramagnetic ions can be detected.

5. Results

The mean susceptibilities of all the samples indicate that they belong to the diamagnetic–paramagnetic phases (Fig. 2), with the majority belonging to the diamagnetic phase (Table 1; sites RT5, RT7, RT9–12, and RT14–18). Three distinct groups were characterized based on the mean susceptibility values, k_m . Group A includes samples with negative mean susceptibility values between -13 and -4×10^{-6} (SI) and belongs to the diamagnetic phase; Group B includes samples with mean susceptibility values between 4 and 30×10^{-6} (SI) and belongs to the very weak paramagnetic phase; and Group C includes samples with mean

susceptibility values greater than 30×10^{-6} (SI) and belongs to the paramagnetic phase. Rock-magnetic experiments indicate the presence of small amounts of magnetic sulphides and magnetites in the limestone rocks (see [Supplementary data item #1](#)).

The mean susceptibilities of samples from the Bar Kokhba limestone are low and most of them are negative. Nevertheless, their AMS results were repeated in consecutive measurements and magnetic fields of 300 A/m. The mean values of the samples that passed the *F*-test fall within the 95% confidence ellipses analyzed for all samples, suggesting that all samples can be considered for further analysis (Fig. 3).

Fig. 3 shows the projections of AMS principal axes and their 95% confidence ellipses. The magnetic fabrics are divided into five types, based on the grouping of AMS axes due to internal deformation (e.g., Borradaile and Henry, 1997), and their relation to bedding planes and rigid-body rotation (e.g., Parés and Van der Pluijm, 2003; Evans and Elmore, 2006; Borradaile and Jackson, 2010). The magnetic fabrics of seven sites (RT3, RT10, RT14–17) represent a tectonic fabric, which is associated with dominant internal deformation, and two sites (RT4 and RT9) have additional sub-vertical foliation. The magnetic fabrics of two sites (RT1 and RT2) represent a tectonic fabric associated with weak rigid-body rotation. Four sites (RT5, RT7, RT8 and RT12) have a tectonic fabric associated with dominant rigid-body rotation and weak internal deformation. In the latter tectonic fabric type, the k_1 – k_2 planes represent the tilted bedding whereas the k_3 axes are well grouped and normal to the bedding. The

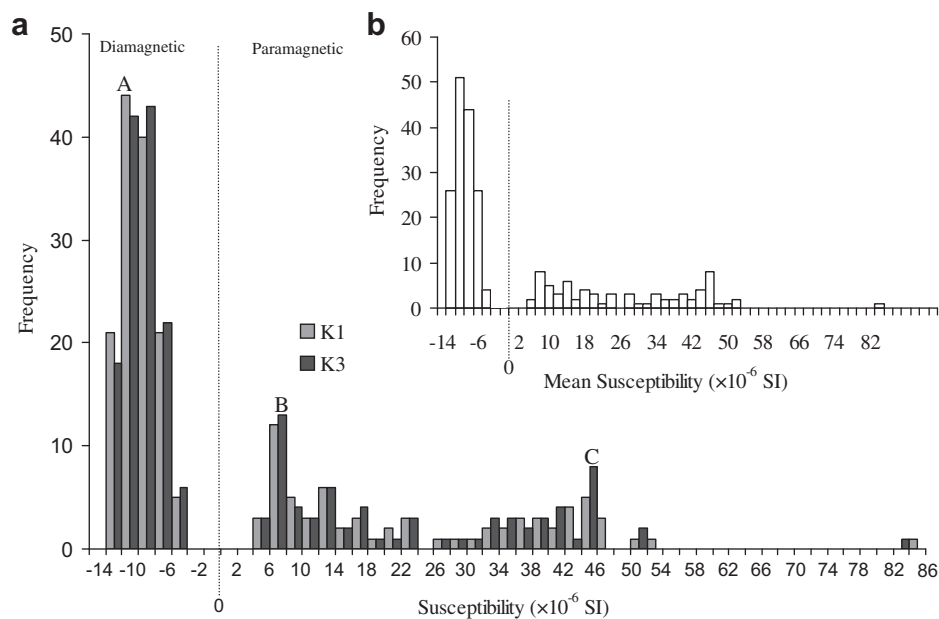


Fig. 2. (a) Frequencies of the principal k_1 and k_3 axes and (b) the mean susceptibilities of the measured samples ($N = 207$). A, B and C mark the histogram picks of the diamagnetic, “very weak” paramagnetic, and “weak” paramagnetic phases, respectively.

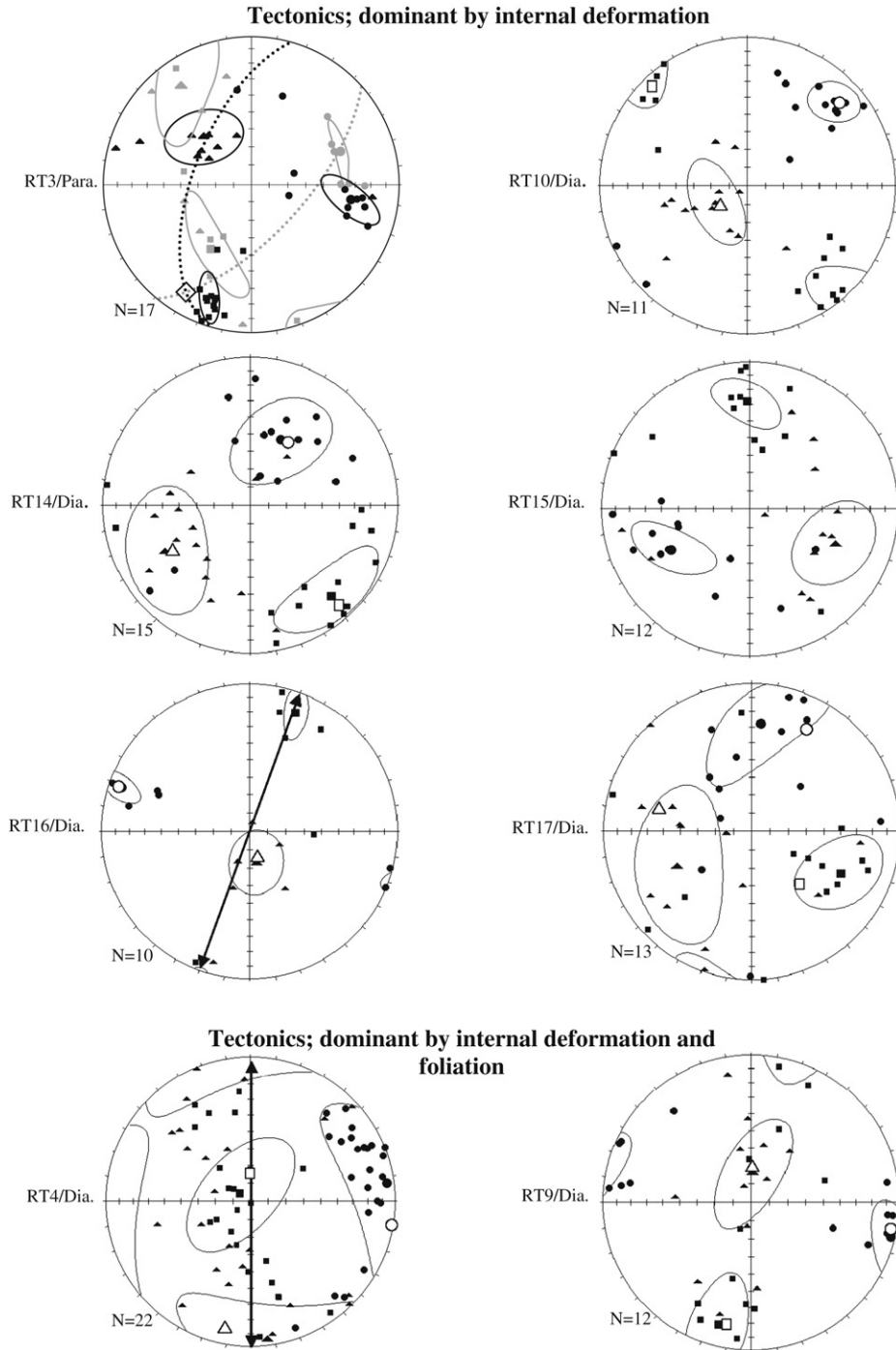


Fig. 3. Lower-hemisphere, equal-area projections of AMS principal axes and the 95% confidence ellipses (Jelinek, 1981); k_1 , k_2 and k_3 axes are marked by solid/open squares, triangles, and circles, respectively. Open symbols represent the mean AMS principal axes that passed the F -test. Diamonds mark fold axes. Dia. – diamagnetic phase; Para. – paramagnetic phase; dotted great circle marks the bedding. Black arrow marks a fault plane. In fold structures (RT2 and RT3), data from opposite flanks are separated by different colors (black and gray).

magnetic fabric of RT11 is rather disperse and is not associated with tectonic fabric. The magnetic fabric of the calcite-filled vein (RT18) shows well-grouped k_3 axes that are perpendicular to the strike of the vein walls. Micrographic study shows that the calcite crystals grew perpendicular to the vein walls along their c -axes, indicating that k_3 axes are parallel to the c -axes.

Three sites, RT1, RT2 and RT3, are located along fold flanks in the Kefar Giladi lacustrine unit and belong to the paramagnetic phase (Table 1; Fig. 1). In RT1 and RT3 the k_1 axes lie parallel to the

NNE–SSW trending fold axes. In RT2 the k_3 axes lie parallel to the NNE–SSW trending fold axis (Fig. 3). Projection of the average k_3 axes of all sites indicates three main groups of trends (Fig. 4): (A) ~W–E (including sites RT4, RT7, RT9 and RT16); (B) ~NW–SE (including sites RT1, RT5 and RT8) and (C) plunging ~NNE (including sites RT10, RT12, RT14 and RT15).

The P' or Δk values and the AMS shape of the diamagnetic samples could change due to a contribution of Fe minerals (e.g., Borradaile and Henry, 1997) and with the addition of Fe^{2+} and

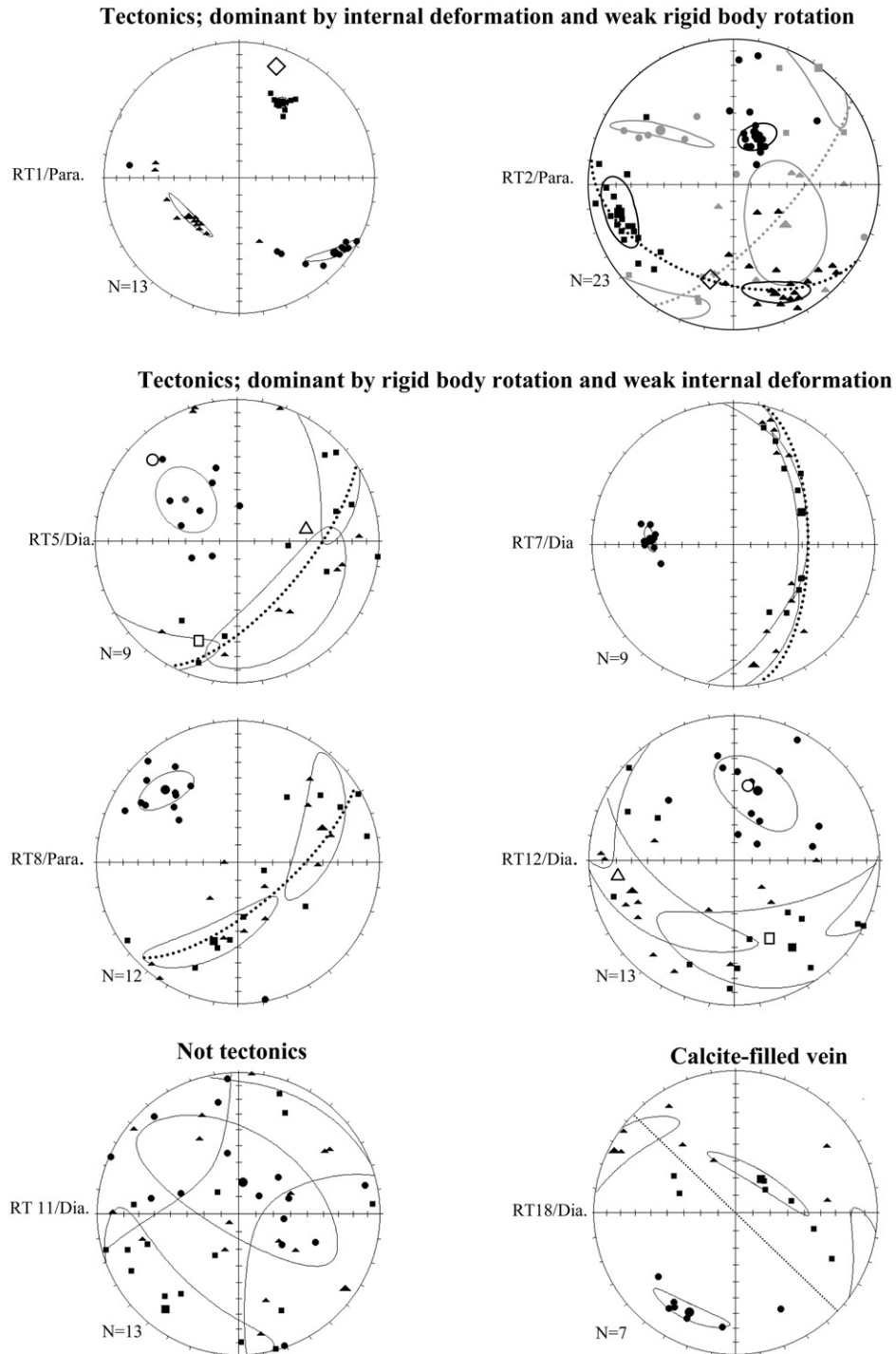


Fig. 3. (continued)

Mn^{2+} ions into the calcite structure (Schmidt et al., 2006; Almqvist et al., 2010). Yet, the comparison between the T and P' parameters shows no correlation. A majority of the diamagnetic samples has positive T values and, hence, are characterized by an oblate shape. The paramagnetic samples have either negative T values and a prolate shape, or very low positive T values and almost a spherical shape (Fig. 5). Fig. 6 shows that all the diamagnetic samples have Fe contents lower than 130 ppm, and there is no dependence between Δk or P' and the Fe content or dependence between Δk and k_m . For

the diamagnetic phase RT11 has the lower value of Δk , around 0.07×10^{-6} (SI), and RT7 has the higher value of Δk , around 0.2×10^{-6} (SI) (Fig. 6a). For the paramagnetic phase, RT8 has the lower value of Δk , around 0.1×10^{-6} (SI), and RT1 has the higher value of Δk , around 0.9×10^{-6} (SI) (Fig. 6a). In RT18 the T parameter is positive, k_1 , k_2 and k_3 have values of -11.6 , -11.66 , -12.39 ($\times 10^{-6}$ (SI)), respectively, and Δk is around 0.8×10^{-6} (SI), suggesting that the vein material behaves as a pure diamagnetic single-crystal calcite.

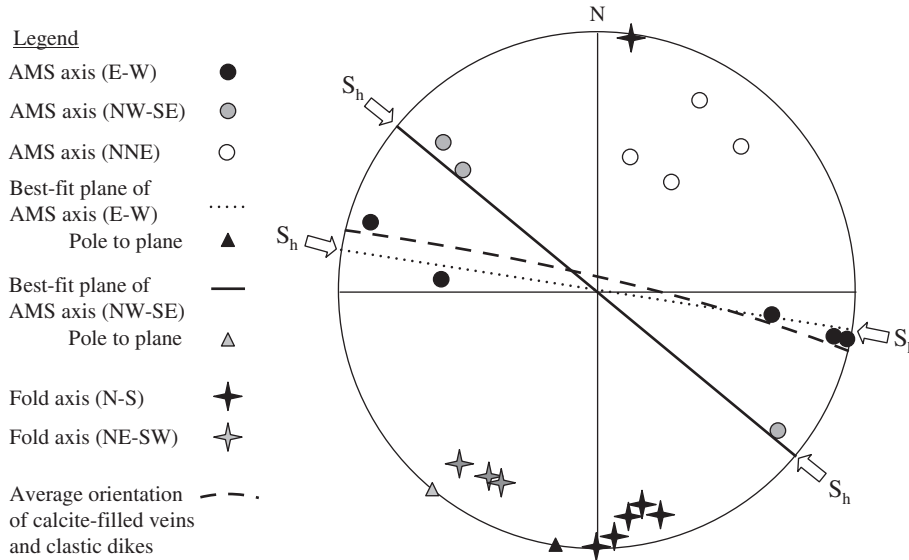


Fig. 4. A summary stereonet comparing the orientations of meso-structures (Weinberger et al., 2009) and AMS axes in the eastern (Metulla) block. Fold axes are derived from averages of fold hinge populations at specific localities, and π diagrams of large folds. The average orientation of veins and clastic dikes are marked by a dashed great circle. AMS axes fall along ~NW–SE or ~W–E striking best fit great circles, which correspond to two distinct phases of shortening axes, S_h . Triangles mark the poles of these great circles and are located close to the two groups of the fold trends.

6. Discussion

6.1. General

The present results were obtained after repeated measurements, especially for those samples that had negative susceptibilities. All measurements were reproducible and, can therefore be considered accurate albeit their low susceptibility values. While not all samples passed the *F*-test, the means of those that did fall within the 95% and the 90% confidence ellipses analyzed for the total samples, suggesting that all samples can be considered for further analysis. Although there is a presence of small amounts of magnetic sulphides and magnetites in the limestone rocks (see Supplementary data item

#1), all the diamagnetic samples have negative principal axes with the average of $k_m \sim -10 \times 10^{-6}$.

Schmidt et al. (2006) suggested that the paramagnetic susceptibility can be quantitatively related to the content of paramagnetic ions. The increase of susceptibility is 0.6×10^{-6} (SI) per 100 ppm Fe and 0.9×10^{-6} (SI) per 100 ppm Mn. Assuming that the ions Fe and Mn of sample RT10-2 (Table 2) are all divalent and replace the Ca^{2+} in the calcite structure, than it would increase the susceptibility by $\sim 1 \times 10^{-6}$ (SI). Because RT10-2 has $k_m = -7 \times 10^{-6}$ and the calculated contribution of the paramagnetic sub-fabrics is not sufficient to explain the difference between k_m of pure calcite (-12×10^{-6}) and the measured -7×10^{-6} of RT10-2, it is suggested that part or all the Fe and Mn ions is situated in the ferromagnetic minerals.

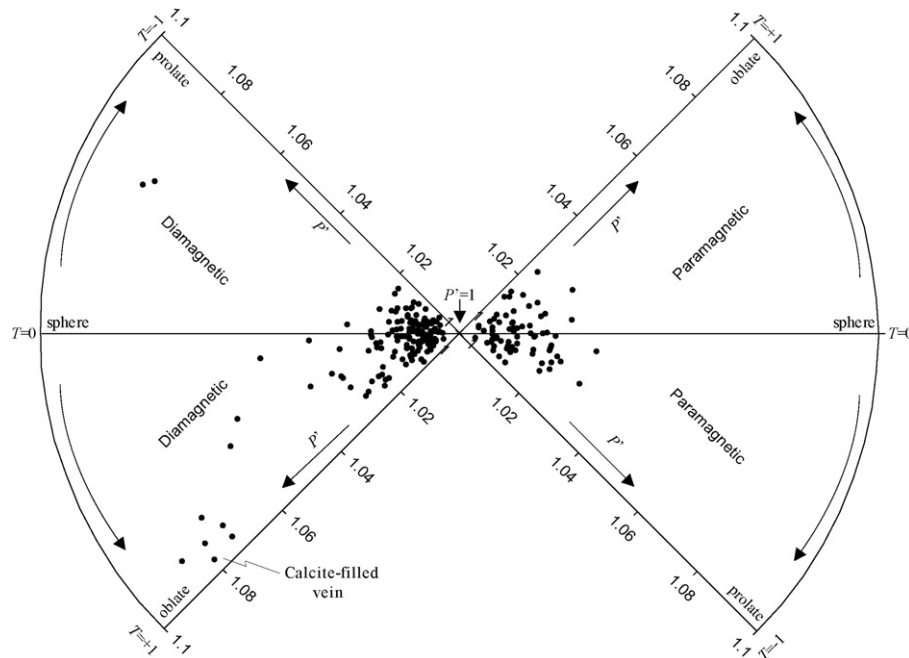


Fig. 5. Corrected anisotropy degree P' and shape parameter T data of diamagnetic and paramagnetic samples from northern Israel presented on a $\pi/4$ segment polar plot. In this plot P' is a radius and T is an arch-length. Plot first introduced by Borradaile and Jackson (2004).

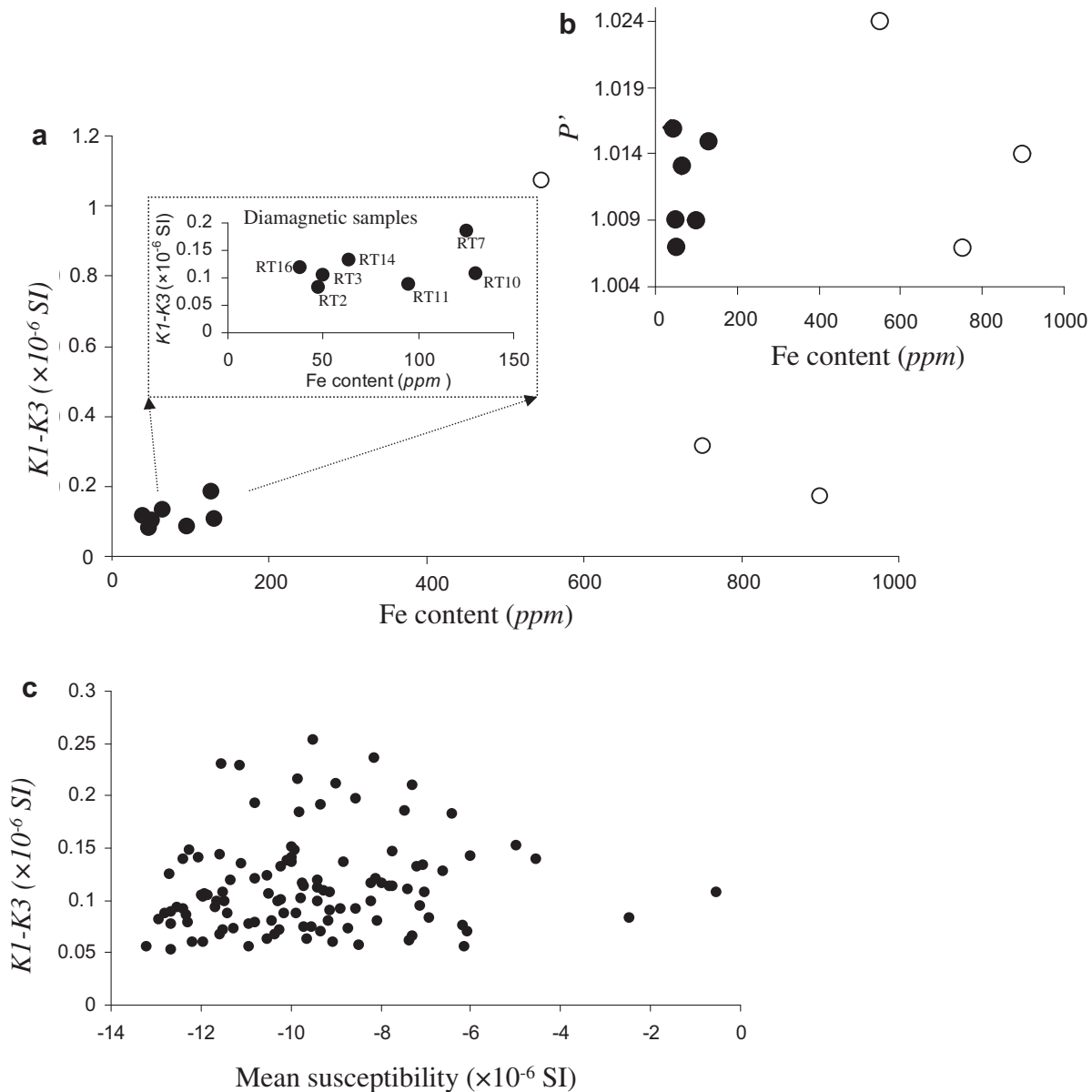


Fig. 6. (a) Susceptibility differences (Δk) versus iron content. (b) the corrected anisotropy degree (P') versus iron content. Solid and open circles mark diamagnetic and paramagnetic samples, respectively.

This conclusion is in agreement with the rock-magnetism experiments (see [Supplementary data item #1](#)).

Borradaile and Jackson (2010) suggested that Fe and Mn ions are the major sources of paramagnetism in minerals. When these magnetic ions are present in non-negligible quantities ($\sim 0.5\%$) their positive susceptibilities outweigh the negative diamagnetic susceptibilities of the bulk rock material. Schmidt et al. (2006) have demonstrated that substitution of Fe^{2+} for Ca^{2+} of more than 500 ppm produces an inverse magnetic fabric. If the magnetic fabric is controlled by both diamagnetic, paramagnetic and/or ferromagnetic sub-fabrics, Δk or P' should depend on the Fe and Mn content of the individual specimens (Schmidt et al., 2006; Almqvist et al., 2010) and on the k_m as well.

In addition, Schmidt et al. (2006) showed that the deviation of the k_3 direction from the c -axis is only within 3.4° if calcite samples have $k_m < -9 \times 10^{-6}$ (SI) (i.e., they are contaminated by small amounts of paramagnetic and ferromagnetic fabrics).

In the present study, the total concentrations of these ions in the Bar Kokhba limestone are less than 0.05% of the bulk rock material.

The iron content of samples from the Bar Kokhba limestone is less than 130 ppm (Table 1 and Fig. 6). However, all their AMS axes (k_1, k_2, k_3) have negative susceptibilities (Figs. 2 and 6). The present results show no dependency between Δk or P' and the Fe/Mn content (Fig. 6) and between Δk or P' and k_m values. Hence, the overall magnetic fabrics are solely controlled by the diamagnetic sub-fabric and the alignment of c -axes of calcite crystals (Almqvist et al., 2010). In addition, the AMS fabric of samples with $k_m < -9 \times 10^{-6}$ is generally similar to that of the AMS fabric of samples with $k_m > -9 \times 10^{-6}$, indicating that the latter group is also controlled by the sub-diamagnetic fabric.

The alignment of the k_3 axes in the diamagnetic Bar Kokhba limestone helps to assess the strain fields prevailing post-deposition and during the tectonic evolution of the DSF. For this

assessment, we also considered samples taken from the paramagnetic Timrat and Kefar Giladi formations.

6.2. Principal strain axes

In calcite-filled veins the *c*-axes are commonly oriented perpendicular to the vein walls (Hudleston and Srivastava, 1997) as are the *c*-axes in RT18. This observation supports the notation that the *k*₃ axes in the diamagnetic rocks are parallel to the *c*-axes. Notably, in calcite-filled veins the *k*₃ axes indicate the “free” growing directions of the calcite crystals into the vein cavity, whereas in deformed sedimentary rocks they indicate the re-orientation direction of the *c*-axes due to strain.

Almost all the analyzed magnetic fabrics evolved due to internal deformation occasionally accompanied by a rigid-body rotation, as indicated by the grouping of the AMS axes and/or their relations to bedding and fold axis (Fig. 3). The obtained shortening axes (i.e., parallel to *k*₃ axes) can be grouped into three sets of directions, namely ~W–E, ~NW–SE and ~NNE-plunging finite shortening axes (Fig. 4). The spatial distribution of the three inferred shortening axes is presented on the foreground of the study area fault map (Fig. 7). The ~W–E shortening axes are distributed throughout the study area and are commonly detected at sites located along fault planes or relatively close to such planes. The ~NW–SE shortening axes are present south of the branching point between the Har Zefiyya and Qiryat Shemona faults; the ~NNE-plunging shortening axes are present north of this point. Fig. 4 shows the shortening axes inferred from the present AMS study together with the ~W–E and ~NW–SE shortening axes inferred previously from meso-scale structures (Weinberger et al., 2009). The orientation of the great circle along which the ~W–E oriented *k*₃ AMS axes lie is very similar to the average plane of the calcite-filled veins and clastic dikes in the study area. The pole of this circle is closely located to the populations of the ~N–S fold axes in the eastern (Metulla) block. The pole of the great circle along which the ~NW–SE oriented *k*₃ axes lie is closely located to the populations of the ~NE–SW fold axes. These observations show a good agreement between finite-strain axes inferred from meso-scale structures and those inferred from *k*₃ axes. Two main observations led Weinberger et al. (2009) to suggest that the ~NW–SE shortening direction predated the ~W–E shortening direction and that the latter has been dominant since the Pleistocene: (1) the Pleistocene Hazbani basalt shows only ~N–S trending folds and lacks ~NE–SW trending folds; and (2) the compatible ~W–E striking veins are younger than 400 kyr (U–Th ages, see Weinberger et al., 2008). Furthermore, the structural analysis provides evidence for the transition from an early (pre-Pleistocene) phase of pure strike-slip motion to a late (Pleistocene to Recent) phase of convergent strike-slip motion and strain partitioning.

Based on this structural analysis, it is suggested that the ~NW–SE *k*₃ axes represent pre-Pleistocene shortening axes and the ~W–E *k*₃ axes, Pleistocene to Recent shortening axes. Noteworthy, three out of four sites in which the magnetic fabric is due to a paramagnetic phase are characterized by ~NW–SE *k*₃ axes (Fig. 7), suggesting that the latest phase of ~W–E shortening did not necessarily reorient the paramagnetic *k*₃ axes.

The mean vector of the diamagnetic *k*₃ axes (034°/31°) of sites RT10, RT12, RT14 and RT17 suggests a ~NNE-plunging shortening axis (Fig. 3). This shortening axis is less understood because it is not directly compatible with the meso-scale structures within the eastern (Metulla) block. The *k*₃ axes may represent an inverse fabric (*k*₁||*c*-axes) for NNE extension. Yet, the inverse fabric (and the NNE extension) is rejected based on the independence of the Δ*k* and the Fe and Mn concentrations (Fig. 6 and Table 1) and the low concentrations of these ions at those sites. Moreover, the ~NNE-plunging shortening axis is not compatible with left-lateral motion along the

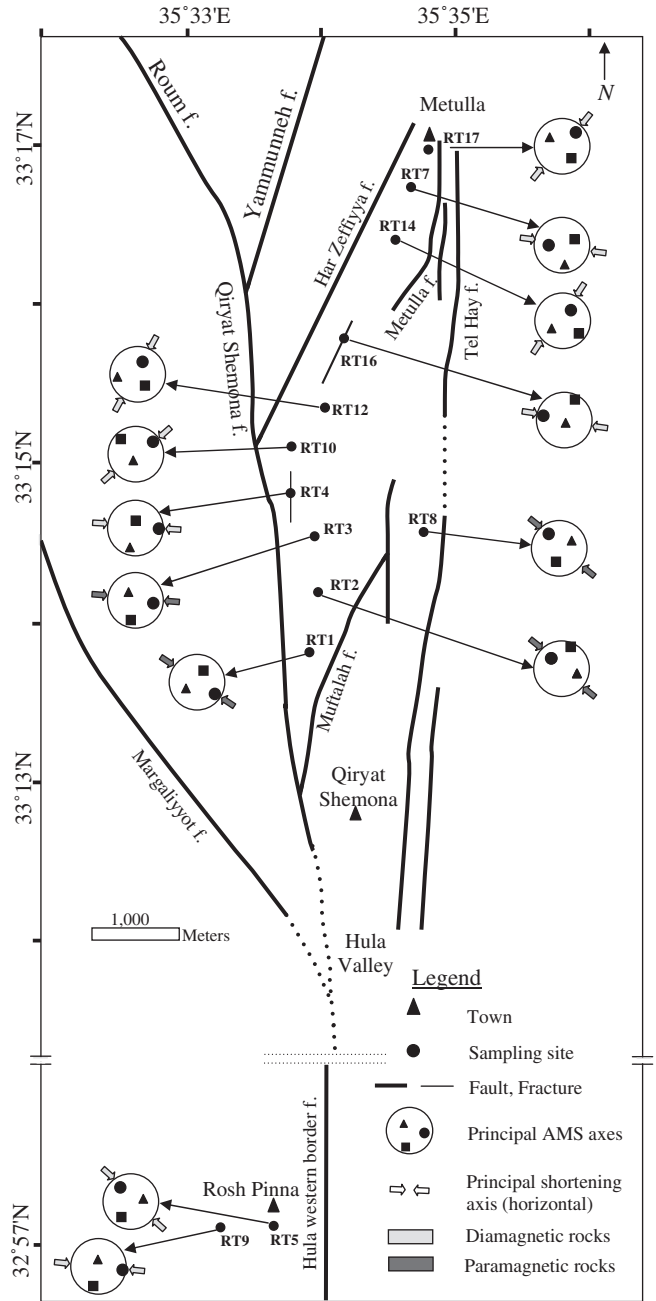


Fig. 7. Map of the main fault segments of the Dead Sea Fault (DSF) in the study area and stereograms of the mean principal AMS axes (see legend in Fig. 3). Arrows mark the inferred (horizontal) shortening directions at the sites studied. The pattern of the arrows marks the type of the dominant fabric (diamagnetic or paramagnetic).

master Qiryat Shemona–Yammunneh faults. Yet, several sites indicate a ~NNE-plunging shortening axis, all of them located within a 400-m wide rock strip parallel to the NNE-striking Har Zefiyya fault. This AMS-based shortening axis is mostly compatible with pure (mode I) extension or oblique normal and left-lateral slip along the Har Zefiyya fracture/fault. Hence, the NNE shortening axis seems to be related to an early stage of the DSF branching in this area, in which faults such as Har Zefiyya were initiated as pure mode I fractures. Within the 400-m wide rock strip parallel to the Har Zefiyya fault, four sites (RT10, RT12, RT14, and RT17) apparently preserved a magnetic fabric that originated in the earliest tectonic phase (~NNE-plunging shortening), while three sites (RT4, RT16, and RT7)

preserved the latest tectonic phase of \sim E–W shortening. These sites are all located along a zone of highly localized strain (i.e., fault plane or fault zone), suggesting that the diamagnetic k_3 axes were selectively reoriented in those sites by the latest \sim W–E shortening.

Based on the above discussion, we suggest that the principal strain axes in northern Israel have been changed over time. The earliest \sim NNE-plunging shortening axis prevailed during the early stage of the DSF initiation (i.e., Middle Miocene). The \sim NW–SE shortening prevailed during the Neogene, and the latest \sim W–E shortening prevailed during the Pleistocene to Recent.

6.3. Possible correlation between the anisotropy degree (P'), susceptibility difference (Δk) and strain

The AMS and chemical results strongly suggest that almost all the diamagnetic samples are monomineralic, calcite-bearing rocks (e.g., Figs. 2 and 6). In addition, there is no dependence between P' or Δk and the Fe/Mn content (Fig. 6) as well as between P' or Δk and k_m values. Yet, the diamagnetic samples still have variations in the P' or Δk even when they have similar strong k_m negative values (Figs. 6 and 8 and Table 1). The increase of P' , Δk and k_m values might be the result of an increase of the Fe and Mn contents (paramagnetic ions) within calcite crystals and/or the growth of ferromagnetic inclusions (Almqvist et al., 2010; Borradaile and Jackson, 2010). Alternatively, an increase in the strain magnitude may lead to a better alignment of the c -axes and an increase in P' and Δk values (Hrouda, 2004; Schmidt et al., 2009). These alternatives are discussed below.

The k_m value of calcite-filled vein (RT18) is around -12×10^{-6} (SI), its P' is around 1.08 and the Δk is around 0.8 ($\times 10^{-6}$ (SI)) (Table 1; Fig. 8). These values are very similar to that of a pure single-crystal calcite (e.g., Owens and Rutter, 1978; Rochette, 1988; Evans et al., 2003; Schmidt et al., 2006). The k_m value of RT17 (Bar Kokhba limestone) is -12.6×10^{-6} (SI) similar to that of pure single-crystal calcite. However, its P' and Δk values are 1.004 and 0.08, respectively, much lower than that of RT18 (Fig. 8). A likely explanation for these differences is that the c -axes of RT17 are greatly dispersed compared to those of the well-aligned, wall-normal calcite crystals in the veins. On the other hand, RT7 has the second highest (after RT18) P' and Δk values (1.025 and 0.2, respectively, Fig. 8 and Table 1), yet, it has characteristics of an almost pure calcite crystal (e.g., oblate AMS shape and Fe content of 125 ppm). In RT10, the Fe content is 130 ppm, the k_m is

around -7.1×10^{-6} (SI), P' is 1.015, and Δk is 0.015. RT16 has similar values of Fe content (125 ppm) and k_m (-7.4×10^{-6} (SI)), yet, the values of P' and Δk are higher (1.027, and 0.025, respectively). We attribute these differences of P' and Δk values to a difference in the strain magnitudes. Since the alignment of the c -axes within the host rock depends on the degree of deformation (Hrouda, 2004), RT7, which is located close to the fault plane, may represent the highest strain level among the samples analyzed (Figs. 8 and 9).

On the assumption that the values of RT17 represent an undeformed matrix with $P'a = 1.004$, $\Delta k = \sim 0.08$, the values of RT7 ($P' = 1.025$, $\Delta k = \sim 0.2$) represent deformed matrix by increase of 1.7% of its original degree of anisotropy and 150% of its original susceptibility difference. Hence, in calcite-bearing rocks different P' or Δk values may indicate different strain magnitudes and may be associated with different strain mechanisms.

Variation of P' or Δk values may represent the inelastic strain or the plastic deformation stored in the calcite-bearing rocks (Kapička et al., 2006). Fig. 9 shows the variations of P' values with the distance from major fault planes. These values decrease with the distance from the fault planes, and can be represented by power-law fitting. We suggest that this decrease of P' values is related to the finite inelastic strain accumulated during time of faulting (co-seismic and inter-seismic activities) and several strain phases (e.g., \sim NNE, \sim NNW–SSE and \sim W–E shortening phases in the Metulla block). The lower value of $P' = 1.0067$ is represented in site RT17 at a distance of ~ 230 m from a major fault plane. The highest value of $P' = 1.025$ is represented in site RT7 at a distance of ~ 20 m from a major fault plane. Hence, the maximum difference of P' ($\Delta P'$) values in the Metulla block is on the order of 1.7%.

Noteworthy, $\Delta P'$ of 3% was found for shortening of up to 25% in stressed cylinder tests made by Borradaile and Alford (1988) and for strain gradients in mylonite quartzites (Tripathy et al., 2009). Schmidt et al. (2009) report on Δk of ~ 0.2 for pure calcite deformed under 150 MPa in cold uniaxial pressure. Based on these experiments and assuming that only 50% of the Δk values are due to deformation, the pressure magnitudes represented by the present samples are up to ~ 30 MPa.

Based on the discussion above, it is proposed that the higher P' and Δk values represent the accumulation of inelastic strain that was stored within the host rock around the fault plane during the intense shearing period. This proposal should be elaborated in future works.

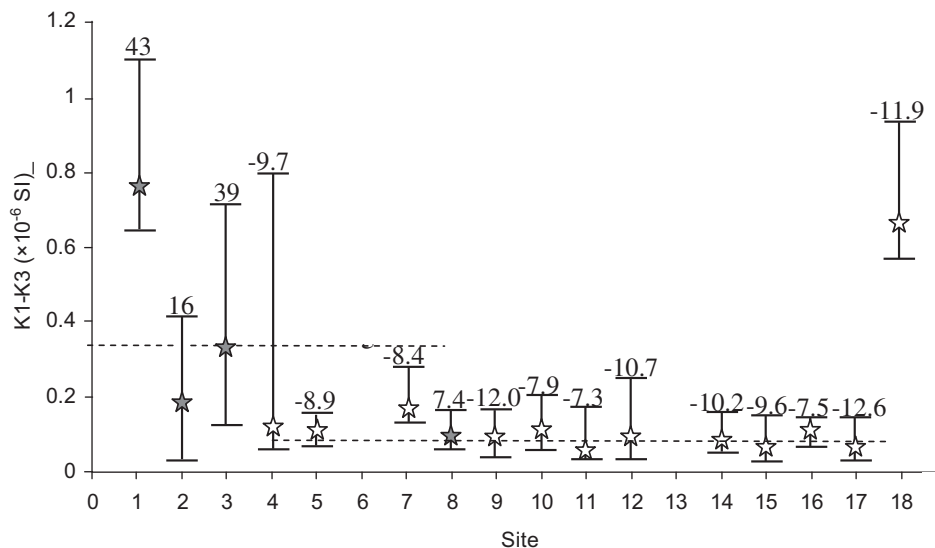


Fig. 8. Distribution of susceptibility differences (Δk) values per sampling site. Gray and white stars mark the average values of Δk for the paramagnetic and diamagnetic samples, respectively. The upper dashed line marks the average Δk of the paramagnetic sites. The lower dashed line marks the average Δk of the diamagnetic sites.

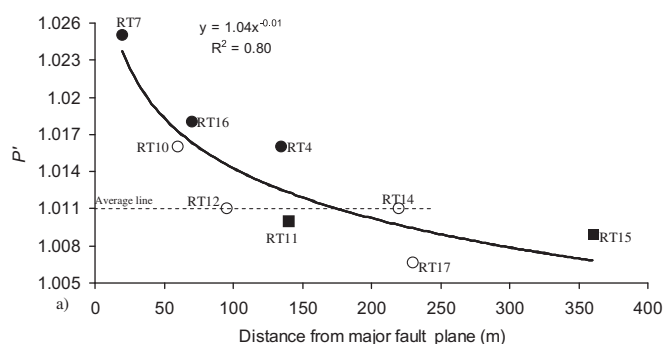


Fig. 9. Variations of P' with distance from the fault planes. Solid and open circles mark sites of \sim W–E and \sim NNE-plunging shortening axes, respectively. Squares mark sites of undetermined shortening axes. See text for details.

6.4. Fold-related AMS variations

Sites RT1, RT2, and RT3 are paramagnetic and dominated by internal deformation due to folding (Table 1, Fig. 3). The vertical layers of RT1 and the $\sim 30^\circ$ inclined RT2 are related to the same set of fold structures. However, in RT1 the k_1 axes are well grouped and lie within the fold plane, indicating elongation parallel to the fold axis, while in RT2 the k_3 axes are well grouped and lie within the fold plane, indicating shortening parallel to the fold axis. In RT3 the k_1 axes are well grouped and parallel to the fold axis, indicating elongation parallel to the fold axis and shortening perpendicular to that direction.

The 90° difference between the directions of the k_3 axes in RT1 and RT2 can be explained by two alternatives: (1) the (internal) state of deformation along the fold structure is heterogeneous due to fold mechanisms such as “bending by orthogonal flexure” or the “buckling by orthogonal flexure” (e.g., see Fig. 16.2 in Twiss and Moores, 1992). This is directly reflected by different directions of the AMS axes at different structural positions within the fold structure; (2) the magnetic fabric of RT1 is “normal” (i.e., c -axes parallel the shortening axis) and that of RT2 is “inverse”, namely, the c -axes are orthogonal to the shortening axis. Note that the possibility of an inverse fabric was rejected for the diamagnetic rocks (see Section 6.1), but was not yet rejected for the paramagnetic rocks.

Inverse fabric in calcite-bearing rocks is mainly formed by contaminating Fe-bearing minerals (Rochette, 1988) or by Fe-rich calcites (Schmidt et al., 2006). In both cases the inverse fabric is indicated by high Fe concentrations and mean susceptibility values, and possibly by a prolate AMS ellipsoid (Schmidt et al., 2006). In addition, the mean susceptibility may increase due to contamination of Fe-bearing minerals. The mean susceptibility of RT1 and RT3 is more than twice greater than the mean susceptibility of RT2 (Table 2). Yet, the Fe and Mn concentrations in RT1 are 545 and 70 ppm, respectively ($\sim 0.18\%$ of the total chemical elements), while these concentrations in RT2 are about 900 and 100 ppm, respectively ($\sim 0.26\%$ of the total chemical elements) (Fig. 8 and Table 1). The shape of the AMS ellipsoid depends on the position of the specimen in the fold (Hrouda, 1978). Indeed, the AMS shape of RT1 is prolate while that of RT2 and RT3 is oblate. Hence, it is unlikely that the difference in the directions of the k_3 axes is due to an inverse fabric. Alternatively, the variation in the directions of the k_3 axes is related to the degree of the internal deformation within the fold structures.

7. Conclusions

The iron content of most samples from the limestone studied is less than 130 ppm, all the AMS principal axes (k_1 , k_2 , k_3) have negative susceptibilities, and the magnetic fabrics are represented

by oblate AMS ellipsoids. Hence, these samples contain magnetic fabrics that are dominated by the diamagnetic phase, which are solely controlled by the alignment of c -axes of almost pure calcite crystals. This alignment helps to assess the strain fields prevailing post-deposition and during the tectonic evolution of the DSF. Based on the present AMS measurements of the diamagnetic as well as a few paramagnetic rocks, three groups of minimum k_3 AMS axes are defined: (1) Group A with \sim NNE-plunging axes; (2) Group B with \sim NW–SE axes; and (3) Group C with \sim E–W axes. The latter two groups of k_3 axes are aligned sub-parallel to finite-strain axes inferred from meso-scale structures (i.e., folds, faults and veins) next to the DSF. This indicates that k_3 axes of diamagnetic rocks can be good proxies for strain field directions near major faults. The \sim NW–SE and the \sim E–W shortening axes are related to the pure left-lateral motion along the DSF during the Neogene, and to contractional strike-slip motion and strain partitioning during the Pleistocene to Recent, respectively. The \sim NNE-plunging shortening axis might be associated with an earlier extensional strain regime along the branching DSF in northern Israel.

The differences between the P' ($\sim 2\%$) and the Δk (~ 0.2) of the diamagnetic rocks are related to differences in strain magnitudes. Based on the proximity of the outcrops to the fault locations, it is suggested that the differences of the P' and Δk values reflect the stored inelastic strain within the calcite matrix due to faulting activity and internal strain heterogeneity within fold structures.

The present work strengthens the suggestion of Schmidt et al. (2006) that good AMS results can be obtained from calcite-bearing rocks when their mean susceptibility is negative.

Acknowledgments

This study was supported by grant no. 2004232 from the United States-Israel Binational Science Foundation (BSF) and the Israeli Ministry of National Infrastructures. We are indebted to the Editor, Joao Hippertt, Graham Borradaile and anonymous reviewer for their thorough and very helpful reviews. We are grateful to Michael Gross, Ann Hirt, Meir Abelson, Hagai Ron, Ron Shaar, Avner Ayalon and Yehuda Eyal for fruitful discussions during the course of this study. The structural data were plotted using Rick Allmendinger's program *Stereonet*.

Appendix. Supplementary data

Supplementary data associated with this article can be found in the online version, at doi:10.1016/j.jsg.2011.02.001.

References

- Abelson, M., Baer, G., Agnon, A., 2001. Evidence from gabbro of Troodos ophiolite for lateral magma transport along a slow-spreading mid-ocean ridge. *Nature* 409, 72–75.
- Almqvist, B.S.G., Hirt, A.M., Schmidt, V., Dietrich, D., 2009. Magnetic fabrics of the Morcles Nappe complex. *Tectonophysics* 466, 89–100.
- Almqvist, B.S.G., Herwegh, M., Schmidt, V., Pette, T., Hirt, A.M., 2010. Magnetic susceptibility as a tool to study deformed calcite with variable impurity content. *Geochemistry, Geophysics, Geosystems* 11, Q01209. doi:10.1029/2009GC002900.
- Baer, G., 1995. Fracture propagation and magma flow in segmented dykes: field evidence and fabric analyses, Makhtesh Ramon, Israel. In: Baer, G., Heimann, A. (Eds.), *Physics and Chemistry of Dykes*. Balkema Publisher, Rotterdam, pp. 125–140.
- Beydoun, Z.R., 1977. Petroleum prospects of Lebanon. *American Association of Petroleum* 61, 43–64.
- Borradaile, G.J., 1987. Anisotropy of magnetic susceptibility: rock composition versus strain. *Tectonophysics* 138, 327–329.
- Borradaile, G.J., 1988. Magnetic susceptibility, petrofabrics and strain. *Tectonophysics* 156, 1–20.
- Borradaile, G.J., 1991. Correlation of strain with anisotropy of magnetic susceptibility (AMS). *Pure and Applied Geophysics* 135, 15–29.
- Borradaile, G.J., Alford, C., 1988. Experimental shear zones and magnetic fabrics. *Journal of Structural Geology* 10, 895–904.

- Borradaile, G.J., Henry, B., 1997. Tectonic applications of magnetic susceptibility and its anisotropy. *Earth Science Reviews* 42, 49–93.
- Borradaile, G.J., Jackson, M., 2004. Anisotropy of magnetic susceptibility (AMS): magnetic petrofabrics of deformed rocks. In: Martín-Hernández, F., Lüneburg, C.M., Aubourg, C., Jackson, M. (Eds.), *Magnetic Fabric Methods and Applications*. The Geological Society of London, Special Publications, vol. 238, pp. 299–360.
- Borradaile, G.J., Hamilton, T.D., 2004. Magnetic fabrics may proxy as neotectonic stress trajectories, Polis Rift, Cyprus. *Tectonics* 23, TC1001. doi:10.1029/2002TC001434.
- Borradaile, G.J., Jackson, M., 2010. Structural geology, petrofabrics and magnetic fabrics. *Journal of Structural Geology* 32, 1519–1551.
- Burmeister, K.C., Harrison, M.J., Marshak, S., Ferré, E.C., Bannister, R.A., Kodama, K.P., 2009. Comparison of Fry strain ellipse and AMS ellipsoid trends to tectonic fabric trends in very low-strain sandstone of the Appalachian fold–thrust belt. *Journal of Structural Geology* 31, 1028–1038.
- Casey, M.S., Rutter, E.H., Schmid, S.M., Siddans, A.W.B., Whalley, J.S., 1978. Texture development in experimentally deformed calcite rocks. In: Gottstein, G., LuEcke, K. (Eds.), *Proceedings 5th International Conference on Textures of Materials*. Springer Verlag, pp. 231–240.
- Daeron, M., Benedetti, L., Tapponnier, P., Sursok, A., Finkel, R.C., 2004. Constraints on the post 25-ka slip rate of the Yammouneh fault (Lebanon) using in situ cosmogenic ³⁶Cl dating of offset limestone-clast fans. *Earth and Planetary Science Letters* 227, 105–119.
- de Wall, H., Bestmann, M., Ullemeyer, K., 2000. Anisotropy of diamagnetic susceptibility in Thassos marble: a comparison between measured and modeled data. *Journal of Structural Geology* 22, 1761–1771.
- Evans, M.A., Lewchuk, M.T., Elmore, R.D., 2003. Strain partitioning of deformation mechanisms in limestones: examining the relationship of strain and anisotropy of magnetic susceptibility (AMS). *Journal of Structural Geology* 25, 1525–1549.
- Evans, M.A., Elmore, R.D., 2006. Fluid control of localized mineral domains in limestone pressure solution structures. *Journal of Structural Geology* 28, 284–301.
- Glikson, Y.A., 1966. The lacustrine Neogene in the Kefar Gil'adi area, northern Jordan Valley. *Israel Journal of Earth Sciences* 15, 85–100.
- Hamilton, T.D., Borradaile, G.J., Lagroix, F., 2004. Sub-fabric identification by standardization of AMS: an example of inferred neotectonic structures from Cyprus. In: Geological Society, London, Special Publications, vol. 238, pp. 527–540.
- Hirt, A.M., Julivert, M., Soldevila, J., 2000. Magnetic fabric and deformation in the Navia–Alto Sil slate belt, northwestern Spain. *Tectonophysics* 320, 1–16.
- Hrouda, F., 1978. The magnetic fabric in some folds. *Physics of the Earth and Planetary Interiors* 17, 89–97.
- Hrouda, F., 1993. Theoretical models of magnetic anisotropy to strain relationship revisited. *Physics of the Earth and Planetary Interiors* 77, 237–249.
- Hrouda, F., 2004. Problems in interpreting AMS parameters in diamagnetic rocks. In: Geological Society, London, Special Publications, vol. 238, pp. 49–59.
- Hrouda, F., Henry, B., Borradaile, G., 2000. Limitations of tensor subtraction in isolating diamagnetic fabrics by magnetic anisotropy. *Tectonophysics* 322, 303–310.
- Hrouda, F., Krejčí, O., Potfaj, M., Stráník, Z., 2009. Magnetic fabric and weak deformation in sandstones of accretionary prisms of the Flysch and Klippen belts of the Western Carpathians: mostly offscraping indicated. *Tectonophysics* 479, 254–270.
- Hudleston, P.J., Srivastava, H.B., 1997. Strain and crystallographic fabric pattern in folded calcite vein: the dependence on initial fabric. In: Sengrupa, S. (Ed.), *Evolution of Geological Structures in Micro-to Macro-scales*. Chapman and Hall, London, pp. 259–271.
- Ihmlé, P.F., Hirt, A.M., Lowrie, W., 1989. Inverse magnetic fabric in deformed limestones of the Morcles nappe, Switzerland. *Geophysical Research Letters* 16, 1383–1386.
- Jelinek, V., 1977. The Statistical Theory of Measuring Anisotropy of Magnetic Susceptibility of Rocks and its Application. *Geophysika*, Brno, pp. 1–88.
- Jelinek, V., 1981. Characterization of magnetic fabric of rocks. *Tectonophysics* 79, 63–67.
- Kapíčka, A., Hrouda, F., Petrovsky, E., Poláček, J., 2006. Effect of plastic deformation in laboratory conditions on magnetic anisotropy of sedimentary rocks. *High Pressure Research* 26, 549–553.
- Kligfield, R.W., Lowrie, W., Pfiffner, O.A., 1982. Magnetic properties of deformed oolitic limestones from the Swiss Alps: the correlation of magnetic anisotropy and strain. *Eclogae Geologicae Helveticae Acta* 75, 127–157.
- Latta, D.K., Anastasio, D.J., 2007. Multiple scales of mechanical stratification and décollement fold kinematics, Sierra Madre Oriental Foreland, northeast Mexico. *Journal of Structural Geology* 29, 1241–1255.
- Levi, T., Weinberger, R., Aifa, T., Eyal, Y., Marco, S., 2006a. Earthquake-induced clastic dikes detected by anisotropy of magnetic susceptibility. *Geology* 34, 69–72. doi:10.1130/G22001.1.
- Levi, T., Weinberger, R., Aifa, T., Eyal, Y., Marco, S., 2006b. Injection mechanism of clay-rich sediments into dikes during earthquakes. *Geochemistry, Geophysics, Geosystems* 7, Q12009 (2), 1–20. doi:10.1029/2006GC001410.
- Liu, B., Saito, Y., Yamazaki, T., Abdeldayem, A., Oda, H., Hori, K., Zhao, Q., 2001. Paleocurrent analysis for the Late Pleistocene–Holocene incised-valley fill of Yangtze delta, China by using anisotropy of magnetic susceptibility data. *Marine Geology* 176, 175–189.
- Mamtani, M.A., Sengupta, A., 2008. Anisotropy of magnetic susceptibility analysis of deformed kaolinite: implications for evaluating landslides. *International Journal of Earth Sciences*. doi:10.1007/s00531-008-0336-x.
- Owens, W.H., Rutter, E.H., 1978. The development of magnetic susceptibility anisotropy through crystallographic preferred orientation in a calcite rock. *Physics of the Earth and Planetary Interiors* 16, 215–222.
- Parés, J.M., van der Pluijm, B.A., Turell, J.D., 1999. Evolution of magnetic fabrics during incipient deformation of mudrocks (Pyrenees, northern Spain). *Tectonophysics* 307, 1–14.
- Parés, J.M., Van der Pluijm, B.A., 2003. Magnetic fabrics and strain in pencil structures of the Knobs Formation, Valley and Ridge Province, US Appalachians. *Journal of Structural Geology* 25, 1349–1358.
- Parés, J.M., Van der Pluijm, B.A., 2004. Correlating magnetic fabrics with finite strain: comparing results from mudrocks in the Variscan and Appalachian Orogens. *Geologica Acta* 2, 213–220.
- Picard, L., 1952. The geology of Kefar-Giladi. *Bulletin of the Israel Exploration Society*, 73–77. “Lif” memorial vol. B (in Hebrew).
- Raposo, M.I.B., McReath, I., D'Agrella-Filho, M.S., 2006. Magnetic fabrics, rock magnetism, cathodoluminescence and petrography of apparently undeformed Bambuí carbonates from São Francisco Basin (Minas Gerais State, SE Brazil): an integrated study. *Tectonophysics* 418, 111–130.
- Rochette, P., 1988. Inverse magnetic fabric in carbonate-bearing rocks. *Earth and Planetary Science Letters* 90, 229–237.
- Rochette, P., Jackson, M., Aubourg, C., 1992. Rock magnetism and the interpretation of anisotropy of magnetic susceptibility. *Reviews of Geophysics* 30, 209–226.
- Schmidt, V., Günther, D., Hirt, A.M., 2006. Magnetic anisotropy of calcite at room-temperature. *Tectonophysics* 418, 63–73.
- Schmidt, V., Hirt, A.M., Rosselli, P., Hernández, F.M., 2007. Separation of diamagnetic and paramagnetic anisotropy by high-field, low-temperature torque measurements. *Geophysical Journal International* 168, 40–47.
- Schmidt, V., Hirt, A.M., Leiss, B., Burlini, L., Walter, J.M., 2009. Quantitative correlation of texture and magnetic anisotropy of compacted calcite–muscovite aggregates. *Journal of Structural Geology* 31, 1062–1073.
- Sneh, A., Weinberger, R., 2003a. Geology of the Metulla quadrangle, northern Israel: implications for the offset along the Dead Sea Rift. *Israel Journal of Earth Science* 52, 123–138.
- Sneh, A., Weinberger, R., 2003b. Geological Map of Israel, Sheet 2-II Metulla, Scale 1:50,000. Geological Survey of Israel, Jerusalem.
- Soto, R., Casas-Sainz, A.M., Villalaín, J.J., Oliva-Urcia, B., 2007. Mesozoic extension in the Basque–Cantabrian basin (N Spain): contributions from AMS and brittle mesostructures. *Tectonophysics* 445, 373–394.
- Tarling, D.H., Hrouda, F., 1993. *The Magnetic Anisotropy of Rocks*. Chapman and Hall, London, 217 pp.
- Tripathy, N.R., Srivastava, H.B., Mamtani, M.A., 2009. Evaluation of a regional strain gradient in mylonitic quartzites from the footwall of the Main Central Thrust Zone (Garhwal Himalaya, India): inferences from finite strain and AMS analyses. *Journal of Asian Earth Sciences* 34, 26–37.
- Twiss, R.J., Moores, E.M., 1992. *Structural Geology*. W.H. Freeman and Company, New York, 532 pp.
- Weinberger, R., Bar-Matthews, M., Gross, M.R., 2008. Preliminary U–Th ages of calcite-filled veins from the Kefar Giladi Quarry. Geological Survey of Israel, Report #TR-GSI/04/08, 8 pp.
- Weinberger, R., Gross, M., Sneh, A., 2009. Evolving contractional deformation along a plate boundary transform: example from the Dead Sea Fault in northern Israel. *Tectonics* 28, TC5005, 19 pp.